Atmos. Meas. Tech. Discuss., 6, 547–586, 2013
www.atmos-meas-tech-discuss.net/6/547/2013/
doi:10.5194/amtd-6-547-2013

Atmospheric Measurement Techniques Discussions

Polar night retrievals of trace gases in the Arctic using the Extended-range Atmospheric Emitted Radiance Interferometer

Z. Mariani[1], K. Strong[1], M. Palm[2], R. Lindenmaier[1,3], C. Adams[1,4], X. Zhao[1], V. Savastiouk[5], C. T. McElroy[6], F. Goutail[7], and J. R. Drummond[8]

[1]Department of Physics, University of Toronto, Toronto, Canada
[2]Department of Physics, University of Bremen, Bremen, Germany
[3]Physics Division, Los Alamos National Laboratory, Los Alamos, USA
[4]Department of Physics & Engineering, University of Saskatoon, Saskatoon, Canada
[5]Full Spectrum Science Inc., Toronto, Ontario, Canada
[6]Department of Earth & Space Science and Engineering, York University, Toronto, Ontario, Canada
[7]LATMOS, CNRS-Universite Versailles St. Quentin, Guyancourt, France
[8]Department of Physics & Atmospheric Science, Dalhousie University, Halifax, NS, Canada

Received: 4 December 2012 – Accepted: 7 January 2013 – Published: 16 January 2013

Correspondence to: Z. Mariani (zmariani@atmosp.physics.utoronto.ca)

Published by Copernicus Publications on behalf of the European Geosciences Union.

AMTD
6, 547–586, 2013

Abstract

The Extended-range Atmospheric Emitted Radiance Interferometer (E-AERI) was installed at the Polar Environment Atmospheric Research Laboratory (PEARL) at Eureka, Nunavut, Canada in October 2008. Spectra from the E-AERI provide information about the radiative balance and budgets of trace gases in the Canadian high Arctic. Measurements are taken every seven minutes year-round, including polar night when the solar-viewing spectrometers at PEARL are not operated. This allows E-AERI measurements to fill the gap in the PEARL dataset during the four months of polar night. Measurements were taken year-round in 2008–2009 at the PEARL Ridge Lab, which is 610 m above sea-level, and from 2011-onwards at the Zero-Altitude PEARL Auxiliary Lab (0PAL), which is 15 km from the Ridge Lab at sea level. Total columns of O_3, CO, CH_4, and N_2O have been retrieved using a modified version of the SFIT2 retrieval algorithm adapted for emission spectra. This provides the first nighttime measurements of these species at Eureka. Changes in the total columns driven by photochemistry and dynamics are observed. Analyses of E-AERI retrievals indicate accurate spectral fits (root-mean-square residuals $< 1.5\,\%$) and a 10–15 % uncertainty in the total column, depending on the trace gas. O_3 comparisons between the E-AERI and a Bruker IFS 125HR Fourier transform infrared (FTIR) spectrometer, three Brewer spectrophotometers, two UV-visible ground-based spectrometers, and a System D'Analyse par Observations Zenithales (SAOZ) at PEARL are made from 2008–2009 and for 2011. 125HR CO, CH_4, and N_2O columns are also compared with the E-AERI measurements. Mean relative differences between the E-AERI and the other spectrometers are 1–14 % (depending on the gas), which are less than the E-AERI's total column uncertainties. The E-AERI O_3 and CO measurements are well correlated with the other spectrometers; the best correlation is with the 125HR ($r > 0.92$). The 24-h diurnal cycle and 365-day seasonal cycle of CO are observed and their amplitudes are quantified by the E-AERI (6–12 % and 46 %, respectively). The seasonal variability of H_2O has an impact on the retrievals, leading to larger uncertainties in the summer months. Despite increased

AMTD
6, 547–586, 2013

water vapour at the lower-altitude site 0PAL, measurements at 0PAL are consistent with measurements at PEARL.

1 Introduction

Ground-based Fourier transform infrared (FTIR) spectrometers are deployed across the globe to make measurements of atmospheric composition by absorption and emission spectroscopy. The Extended-range Atmospheric Emitted Radiance Interferometer (E-AERI) is a moderate resolution (1 cm^{-1}) FTIR spectrometer for measuring the absolute downwelling infrared emission from the atmosphere between 400 and 3000 cm^{-1}. The large number of trace gases that have emission features in the infrared enable simultaneous measurements of different trace gases from the ground. For instance, the ability to use Atmospheric Emitted Radiance Interferometer (AERI) measurements to retrieve CO total column concentrations with high sensitivity to the lower troposphere has recently been demonstrated (Yurganov et al., 2010).

The Canadian Network for the Detection of Atmospheric Change (CANDAC) has equipped the Polar Environment Atmospheric Research Laboratory (PEARL), which is located at Eureka, Nunavut (80° N, 86° W), with several spectrometers that measure atmospheric composition. One of these instruments is the E-AERI, which is used for studies of the Arctic radiation budget and atmospheric trace gases. Details of the instrument's design, calibration, installation and performance are provided in Mariani et al. (2012). The E-AERI was installed at the PEARL Ridge Lab (610 m a.s.l.) in October 2008 and acquired one year of measurements before being moved 15 km to the Zero-altitude PEARL Auxiliary Lab (0PAL), which is at an altitude of 10 m. The geography surrounding the two measurement sites is seen in Fig. 1. E-AERI total column retrievals of O_3, CO, CH_4, and N_2O from these two measurement sites are discussed in this paper.

The E-AERI started taking measurements of downwelling radiance at 0PAL in February 2011 (where it has since remained operational) to determine concentrations of

AMTD
6, 547–586, 2013

tropospheric trace gases from sea level and to investigate cooling in the 20-micron region. From a climatology of radiosonde water vapour data, 10–20 % (winter–summer) of the water vapour at Eureka resides in the first 610 m, making 0PAL's location essential for future radiative budget and water vapour studies. The difficulty in fitting H_2O emission, however, is a source of error in the E-AERI trace gas retrievals, as will be discussed. The impact of the increased water vapour on trace gas retrievals at 0PAL will be evaluated by comparing them to the retrievals performed at the PEARL Ridge Lab.

There are several other spectrometers installed at PEARL, all of which are solar-absorption instruments. The Bruker IFS 125HR FTIR spectrometer, two UV-visible Ground-Based Spectrometers (GBSs), three Brewer spectrophotometers, and a System D'Analyse par Observations Zenithales (SAOZ) spectrometer were used to compare total column measurements with the E-AERI and are described in more detail in Sect. 2.4. These provide an extensive dataset that will continue to be used to evaluate E-AERI trace gas retrievals during sun-lit months. During night-time conditions (such as the four months of polar night), the E-AERI is the only spectrometer operating at Eureka that can obtain total column measurements of trace gases; hence it will be used to fill a significant gap in the PEARL dataset.

The SFIT2 retrieval code (Pougatchev et al., 1995; Rinsland et al., 1998), which is widely used in the Network for the Detection of Atmospheric Composition Change (NDACC) Infrared Working Group (IRWG) (e.g. the PEARL 125HR retrievals use SFIT2), has recently been modified so that it can be applied to infrared emission spectra, such as those recorded by the E-AERI. This new emission version of SFIT2 will be implemented in the next version of the code, SFIT4. E-AERI total column retrievals of O_3, CO, CH_4 and N_2O have been performed year-round using this new version of SFIT2.

Eureka is an excellent location for various scientific studies, ranging from polar ozone depletion, to satellite validation, to characterizing long-range transport. The conditions in the Arctic atmosphere can be favorable for the heterogeneous reactions that deplete

AMTD
6, 547–586, 2013

stratospheric O_3 in the cold Arctic polar vortex. N_2O is an important greenhouse gas and has been shown to be the most important ozone-depleting substance emitted today (Ravishankara et al., 2009). Measurements of O_3 and N_2O, particularly during the winter-time formation of the polar vortex, can provide insight into chemical and dynamical processes occurring in this rapidly changing region. Such monitoring at Eureka started in 1993 with the installation of a Bomem DA8 FTIR by Environment Canada (Fast et al., 2011) with regular intensive monitoring using the 125HR (and other) spectrometers beginning in 2006 after the establishment of PEARL (Fraser et al., 2009; Batchelor et al., 2009). PEARL is uniquely situated in close proximity to frequent overpasses by satellites, such as the Atmospheric Chemistry Experiment (ACE), making ground-based measurements at this site particularly useful for satellite validation purposes (Batchelor et al., 2010; Adams et al., 2012a). The products of biomass burning over northern Eurasia, which has increased significantly over the past 100 yr due to human activities, can also be transported to the Arctic and result in CO total column enhancements (Stohl, 2006; Warneke et al., 2010). This provides a growing source of chemically and radiatively active gases such as CO_2, CH_4 and other hydrocarbons that can be measured by ground-based spectrometers such as the E-AERI. Photochemistry has a noticeable effect on the budget of trace gases above Eureka: 24-h darkness (polar night) occurs from mid-October to mid-February and rapidly transitions to 24-h sunlight (polar day) from late-April to late-August. The seasonal variability of these trace gases can be measured by the E-AERI at PEARL; for instance, the polar vortex is frequently above Eureka in the spring, with vortex dynamics playing a key role in the ozone budget, whereas in the summer the variability in trace gases is largely dependent on transport from lower latitudes.

This paper describes the new emission version of SFIT2 and its application, outlines AERI trace gas retrievals using SFIT2 (which is applicable to all other AERIs deployed across the globe), and provides the first continuous polar night trace gas measurements at Eureka. E-AERI measurements and modifications to the SFIT2 retrieval algorithm are discussed in Sect. 2. Section 3 outlines the retrieval methodology, including

AMTD
6, 547–586, 2013

the spectral regions of interest ("miniwindows") and error analysis. Results from E-AERI trace gas measurements made at the PEARL Ridge Lab from October 2008 to September 2009 are shown in Sect. 4; results from measurements at 0PAL from February to December 2011 are shown in Sect. 5. Comparisons with the other spectrometers at PEARL, as well as an investigation of the diurnal and interannual variability of these trace gases above Eureka are provided in these two sections. A summary and conclusions are given in Sect. 6.

2 Measurements

2.1 E-AERI radiances

The E-AERI measures zenith-sky thermal emission from the atmosphere using ABB's MR-300 series Fourier transform spectrometer with a maximum optical path difference of 1 cm, providing an unapodized resolution of 1 cm^{-1}. Its measured radiances have undergone several performance evaluations, including comparisons with other AERI systems at the University of Wisconsin and PEARL, as well as model simulations to ensure measurement reliability (Mariani et al., 2012). The E-AERI operated continuously at the PEARL Ridge Lab from 22 October 2008 to 20 September 2009, except when precipitation occurred, during instrument maintenance, and when a software error caused the hatch to close erroneously (which has since been fixed).

No measurements were made in 2010; during this time the E-AERI was removed from the PEARL Ridge Lab and installed in the same thru-wall configuration at 0PAL, while the Stirling-cycle cooler used on the detector was upgraded to a new THALES Stirling-cycle cryogenic cooler, the sensor-controller digital multimeter was re-calibrated by its manufacturer (Agilent), and the entire instrument underwent calibration and re-certification testing according to the University of Wisconsin Space Science and Engineering Centre's (UW-SSEC) standards and procedures. This ensured the instrument's specifications and performance at 0PAL matched those at PEARL.

AMTD
6, 547–586, 2013

Measurements at 0PAL started on 16 February 2011 and continue to this day. In 2011, there were three periods with no measurements due to instrument issues and maintenance. The instrument was re-certified according to UW-SSEC standards during a service visit in November 2011 to once again ensure instrument performance stability and measurement reliability.

The E-AERI is fully automated and produces 248 co-added spectra every seven minutes except during precipitation events, when the scene-view hatch is automatically closed. For this work, spectra collected in a one-hour window are averaged to produce a dataset of hourly-averaged radiances to improve the signal-to-noise ratio; typically eight spectra are averaged in a one-hour window. Retrievals of trace gases when clouds are present are difficult due to the increased emission from cloud particles, causing a large increase in baseline radiance (Mariani et al., 2012). This increased emission dwarfs the spectral signature from the trace gases of interest. Thus cloudy measurement periods are filtered using a maximum radiance tolerance criterion, which is season-dependent, in the cloud-sensitive region (750–1200 cm^{-1}). The accuracy of the cloud-filtering process has been confirmed by cross-checking with the Millimetre Cloud Radar and meteorological observations at Eureka. Thus all measurements of trace gases presented here were recorded during clear-sky conditions.

2.2 Comparisons to other ground-based emission spectrometers

The E-AERI has been designed to take emission measurements over a broad region of the infrared spectrum that includes atmospheric trace gas emission lines and the so-called "dirty window" around 400 cm^{-1} where much of the infrared cooling to space occurs. Other ground-based emission spectrometers are used to study the emission spectroscopy of distant stars using near-infrared emission spectrometers (e.g. Waldmann et al., 2012) or are designed to measure different atmospheric trace gases (for instance, millimeter-wave radiometers (MWRs) such as the Kiruna millimeter-wave radiometer (KIMRA); Raffalski et al., 2005). MWRs differ from the E-AERI in that they require their detectors to be cooled to significantly lower temperatures (< 35 K) than

AMTD
6, 547–586, 2013

the E-AERI (< 70 K) in order to detect the faint millimeter-wave emission lines. MWRs typically measure weaker emission signals but have higher spectral resolution than the E-AERI. The E-AERI is also zenith-viewing, permitting measurements directly above the site's location, whereas many emission spectrometers (including some MWRs and older variants of the E-AERI) use a slant path to increase the emission signal. The E-AERI software system performs all necessary data calibration and quality control in real-time and, like most MWRs, is fully automated and can be controlled remotely.

Emission spectrometers can be deployed off the ground and utilize different viewing geometries. For instance, the Michelson Interferometer for Passive Atmospheric Sounding (MIPAS) instrument on Envisat and its balloon-borne version (MIPAS-B) measure vertical profiles of trace gases using infrared limb-emission sounding (Fischer and Oelhaf, 1996). The Spectroscopy of the Atmosphere using Far InfraRed Emission – Airborne (SAFIRE-A) operates in the far-infrared spectral region, making limb sounding observations of atmospheric emission from high altitude aircraft (Bianchini et al., 2003). The Scanning Infrared Gas Imaging System (SIGIS) is a ground-based thermal emission infrared spectrometer that measures volcanic SO_2 and SiF_4. To do this, SIGIS (and other instruments that measure volcanic emissions) uses the radiation of the volcanic gas itself, allowing for continuous monitoring day and night of the volcanic plume (Stremme et al., 2012 and references therein). Compared to the E-AERI, some other ground-based infrared emission spectrometers used in the past, such as the Bruker IFS-120M and the Radiation Exolorer in the Far InfraRed-Prototype for Applications in Development (REFIR-PAD) (Becker and Notholt, 1997; Bianchini et al., 2010), have had a narrower spectral range but greater spectral resolution. For all these instruments, the spectra are calibrated using one or more blackbodies. Where one blackbody is used (such as with MIPAS-B), the instrument views cold space as the cold source and the blackbody as the hot source. Since the E-AERI cannot view cold space from the ground, it uses two blackbodies (ambient and hot) for its calibration. Regardless of the type of retrieval algorithm employed, atmospheric profiles of pressure and temperature from radiosondes are typically used as a priori input profiles. More information

AMTD
6, 547–586, 2013

about the E-AERI (such as its field-of-view, nonlinearity knowledge, blackbody characterization, etc.) is provided in Table 2 of Mariani et al. (2012).

2.3 SFIT2 emission add-on

SFIT2 is a radiative transfer and profile retrieval algorithm based on the optimal estimation method (OEM) of Rodgers (1976, 1990, 2000). It produces a calculated spectrum that is fitted to an observed spectrum by adjusting the trace gas volume mixing ratio profiles (Pougatchev et al., 1995; Rinsland et al., 1998). The forward model is a multi-species, multilayer, line-by-line radiative transfer model. The model assumes the Voigt lineshape function, local thermodynamic equilibrium, and homogeneous layers of the atmosphere. SFIT2 is widely used in the infrared remote sounding community and has undergone extensive validation exercises (e.g. Hase et al., 2004). SFIT2 can be used in conjunction with FTIR spectra to retrieve over 25 trace gases, while a maximum of nine interfering species can be included in the retrieval's microwindow.

The SFIT2 retrieval code (along with its predecessors) was designed to use solar absorption measurements from an FTIR as input to the forward model. Hence modifications to the original SFIT2 (v. 3.93) code were required in order to adapt the algorithm to be used with emission spectra, such as those produced by the E-AERI. In this new emission add-on (SFIT2 v. 3.93+Emission), the retrieval code has been modified with an extension to calculate the full radiative transfer. The radiative transfer is given by:

$$\frac{\mathrm{d}I}{\mathrm{d}z} = -\alpha(z)\cdot(I - S) \tag{1}$$

where α denotes the absorption at a given altitude (z), I denotes the radiance, and S denotes the source term. Neglecting scattering, the source term, S, is given by Planck's function (expressed in $\mathrm{W\,cm^{-2}\,sr^{-1}\,cm}$) for blackbody radiation:

$$S = \frac{2hc^2\tilde{\nu}^3}{e^{\left(\frac{hc\tilde{\nu}}{k_B T}\right)} - 1} \tag{2}$$

AMTD
6, 547–586, 2013

where h denotes Planck's constant, c denotes the speed of light, k_B denotes Boltzmann's constant, T denotes the absolute temperature and $\tilde{\nu}$ denotes the wavenumbers (cm^{-1}). In integral form, Eq. (1) is:

$$I(z) = S(z_\infty)e^{-\tau(0,z_\infty)} + \int_\infty^0 S(z) \cdot \frac{de^{-\tau(0,z)}}{dz} dz \quad (3)$$

where $\tau(0, z_\infty)$ denotes the opacity from the ground to the top of the atmosphere, $\tau(0, z)$ denotes the opacity of the layer z to the observer at 0, $S(z_\infty)$ is the source term for the background (top of atmosphere) radiation, and $S(z)$ is the source term of the layer z. While in solar absorption spectroscopy the right most term in Eq. (3) can be neglected due to the negligible emission of the atmosphere compared to the sun, in emission spectroscopy this is the main source of radiation. The numerical iteration scheme used to find the zero of the gradient of the cost function in the OEM has also been changed from Gauss–Newton to Levenberg–Marquardt, which is more efficient with nonlinear solutions where the true solution is sufficiently far from the current iteration point (a priori).

2.4 Comparison datasets

The Bruker 125HR FTIR spectrometer is a NDACC instrument that has been used to make solar-absorption measurements at the PEARL Ridge Lab since 2006 and has been compared with other datasets in several studies (Batchelor et al., 2009; Lindenmaier et al., 2010; Adams et al., 2012a). The 125HR provides partial and total column measurements of many trace gases during sun-lit months, including the four gases that can be measured by the E-AERI. The viewing geometry of the Bruker is a sun-pointing slant path. 125HR total column errors (S_{tot}, comprising the smoothing error, measurement error, interference error, and forward model parameter error) are 4.3 % for O_3, 1.8 % for CO, 14.0 % for CH_4, and 3.9 % for N_2O (Lindenmaier, 2012), which are smaller than those of the E-AERI (10–15 %, as shown in Sect. 3.3).

AMTD
6, 547–586, 2013

The remaining solar-absorption spectrometers at PEARL have been involved in numerous validation campaigns and provide total columns of O_3, and other trace gases. Three Environment Canada Brewer spectrophotometers (#021, #192, #069) deployed on the roof of the PEARL Ridge Lab use direct and scattered sunlight at UV wavelengths (Savastiouk and McElroy, 2005). The viewing geometry of the Brewer spectrophotometers is a sun-pointing slant path, like the 125HR. The standard Brewer algorithm was used to analyze Brewer data, with small changes to the analysis parameters (e.g. the ozone layer was set at 18 km instead of 22 km to better reflect conditions in the Arctic) (Lam et al., 2007). The random error in Brewer total O_3 measurements is typically less than 1 % (Savastiouk and McElroy, 2005).

The two UV-visible GBSs (both NDACC-certified) are very similar instruments and their measurements of zenith-scattered sunlight were analyzed using the same settings to retrieve O_3 total columns (Fraser et al., 2009; Adams et al., 2012a,b). The two GBSs agree within 1 % of each other and the total error of the O_3 column is 6.2 % (Adams et al., 2012a). An NDACC-certified SAOZ UV-visible grating spectrometer (Pommereau and Goutail, 1988) deployed on the roof of the PEARL Ridge Lab took zenith-sky measurements during the spring. The estimated error for SAOZ total O_3 measurements is 5.9 % (Hendrick et al., 2011). GBS and SAOZ total columns were retrieved independently, following NDACC guidelines, using the Differential Optical Absorption Spectroscopy (DOAS) technique (Platt and Stutz, 2008). Both the GBSs and SAOZ are zenith-viewing and use scattered sunlight at sunrise/sunset to make measurements pointing to the azimuth angle of the sun (which varies with the time of year).

3 Methodology

3.1 Retrieval methodology

In order to retrieve total columns of trace gases from E-AERI spectra, the SFIT2 retrieval algorithm is used in conjunction with the High Resolution Transmission Molecular

AMTD
6, 547–586, 2013

Absorption Database (HITRAN) 2008 (Rothman et al., 2009). Refractive ray-tracing and airmass path calculations are computed using the FASTCODE (also referred to as FSCATM) algorithm (Meier et al., 2004). With the OEM, the retrieved profile can be expressed as a linear combination of the a priori and the true state with error contributions. Due to the relatively low spectral resolution of the E-AERI, profile-scaled retrievals were performed (rather than full profile retrievals) in which the entire a priori profile of the trace gas is uniformly shifted (increased/decreased) to match the true state. By definition, scaled retrievals have degrees of freedom for signal = 1 and provide only the total column concentration. Attempts to perform retrievals on a multi-layer grid resulted in convergence problems, likely due to the lack of vertical sensitivity in the lower-resolution E-AERI spectra.

The a priori volume mixing ratio (VMR) profiles for the target trace gas, a priori covariance matrix, $\mathbf{S}_a$, and a priori interfering species VMR profiles are required inputs for the OEM. A priori estimates of trace gas VMR profiles at Eureka have been provided for 64 trace gases and used in previous studies involving SFIT2 retrievals (Batchelor et al., 2009; Lindenmaier et al., 2010). These profiles were produced from a climatology of satellite, ground-based, model, and balloon measurements. The a priori covariance matrix, $\mathbf{S}_a$, which constrains the retrieval to the a priori, was set to 30 % for each target gas. The interfering species covariance matrices were set to 100 %, with the exception of H_2O, which was set to 300 % due to the large seasonal variability of H_2O at Eureka. Daily profiles of pressure and temperature were obtained from a combination of three sources: two daily launches of radiosondes at Eureka were averaged to provide information up to 35 km above Eureka, the National Centre for Environmental Prediction (NCEP) analyses from the NASA Goddard Space Flight Centre provided information from 35–50 km, and the 1976 US Standard Atmosphere was used above 50 km.

The signal-to-noise ratio (SNR) is used to determine the measurement noise covariance matrix, $\mathbf{S}_\varepsilon$, where the diagonals are set to $1/(\mathrm{SNR})^2$. Underestimating the retrieval's SNR causes high root-mean-square (RMS) residuals in the spectral fit, while over-estimating SNR forces the retrieval to fit spectral noise. An estimate of the

AMTD
6, 547–586, 2013

instrument's noise is based on instrument RMS Noise Equivalent Spectral Radiance (NESR) tests performed by UW-SSEC (Mariani et al., 2012). The designated SNR is determined by plotting the "trade-off curve" of the RMS error versus SNR for each gas (test retrievals using a range of SNRs from 2–200 for each gas were performed). A SNR is selected near the elbow of this trade-off curve and ensures that the measurements are not being over-fitted. This technique is described in more detail in Rodgers (2000) and has been used in previous studies (e.g. Batchelor et al., 2009).

3.2 Miniwindows

Due to the lower spectral resolution of the E-AERI, the spectral regions that SFIT2 uses to fit the trace gas spectral lines must be significantly larger than those typically used in fitting high-resolution solar absorption spectra to incorporate sufficient spectral lines of the target trace gas. Since these fitted spectral regions are wider (10–25 times) than the standard microwindows used in NDACC IRWG SFIT2 retrievals, they will be referred to as "miniwindows". A comparison of possible miniwindows was performed for each target trace gas species in order to obtain the lowest fitted RMS residual while permitting retrieval convergence. Attempts were made to avoid spectral regions that have large H_2O emission features due to their large variability and capacity to dwarf emission features of the target gas. The H_2O continuum (resulting from numerous strong H_2O lines up to 700 cm^{-1}) in particular was avoided as much as possible due to the difficulty in its characterization. The a priori VMR profiles of the interfering species were scaled simultaneously with the target trace gas during the retrievals. SFIT2 can incorporate a maximum of nine interfering species for each miniwindow, which, in effect, places a limit on the maximum size of the miniwindow. Table 1 lists the optimal miniwindow selected for each trace gas, the interfering species included in the retrieval, the selected SNR (described in Sect. 3.1), and the typical RMS residual in the spectral fit.

Examples of the spectral fits and residuals for each trace gas listed in Table 1 are shown in Fig. 2. These fits were performed on spring (4 April 2009) hourly-averaged E-AERI spectra and are typical for this time of year. The spectral fits change depending

AMTD
6, 547–586, 2013

on the season; for instance, larger emission features are found in the summer (e.g. large H_2O emission lines due to increased H_2O vapour) compared to the winter. Due to the difficulty in accurately fitting H_2O spectral lines, this slightly increases the RMS residual in the summer months (May–July) and decreases the RMS residual in the winter months (December–February). Meteorological events (i.e. ice clouds, fog, etc.) do not impact spectral fitting due to the cloud-filtering performed prior to the SFIT2 retrievals (described in Sect. 2.1).

3.3 Error analysis

The uncertainty in the measured total columns is determined following the method described in Rodgers (2000), which has been demonstrated for the PEARL 125HR SFIT2 retrievals (Batchelor et al., 2009). Under this approach, the smoothing error (due to interpolation), S_s, and measurement error (due to noise), S_m, are added in quadrature with the forward model parameter errors and interference errors. The noise equivalent spectral radiance (NESR) quantifies the radiometric calibration error of $< 0.4\,\mathrm{mW\,m^{-2}\,sr^{-1}\,cm}$ for 420–1400 $\mathrm{cm^{-1}}$ and $< 0.015\,\mathrm{mW\,m^{-2}\,sr^{-1}\,cm}$ for 2000–2600 $\mathrm{cm^{-1}}$. The radiometric calibration absolute accuracy is $< 1\,\%$ of the ambient blackbody radiance. Forward model errors are determined using a perturbation method for temperature, S_{temp}, and the largest estimates of the uncertainties provided in HITRAN, S_{lint} (line intensity) and S_{lwidth} (air-broadened half-width) (Rothman et al., 2009). A conservative estimate of 20 % was used where the uncertainty in the line parameters was unknown (e.g. O_3 line intensity). The maximum uncertainty within the quoted range from the radiosonde manufacturer (Vaisala) was used as the uncertainty associated with the atmospheric profiles of pressure (±1 hPa) and temperature (±0.5 K). In determining S_{temp} via perturbation, the uncertainties provided in the NCEP profiles were used (a more conservative estimate of 2 K was used below 30 km, 5 K between 30–35 km, 6 K between 35–40 km, 7 K between 40–50 km, and 9 K above 50 km). The interference errors, S_{intspec} and S_{intret}, are the errors in the retrieved column due to the other retrieved species and parameters, respectively. The latter includes instrument

AMTD
6, 547–586, 2013

lineshape, wavelength shift, background slope and curvature, phase error and zero level shift; their combination is described in Rodgers and Connor (2003). Since the E-AERI is zenith-viewing, errors in the solar zenith angle (S_{SZA}) are zero. Hence the total error, S_{tot}, can be expressed as:

$$S_{tot} = \sqrt{S_s^2 + S_m^2 + S_{temp}^2 + S_{lint}^2 + S_{lwidth}^2 + S_{intret}^2 + S_{intspec}^2} \quad (4)$$

The uncertainty due to measurement noise (S_m) is considered to be random, and the uncertainty due to spectroscopic parameters (S_{lint} and S_{lwidth}) is mostly systematic, although a clear division between systematic and random uncertainties is not absolute. Thus these errors have been added in quadrature, as recommended by the International Organization of Standardization (1993). Several error sources (S_{intret}, $S_{intspec}$, S_{temp}, and S_s) vary from spectrum to spectrum and can be season-dependent. For instance, the interference from H_2O line-broadening decreases in the winter as the amount of water vapour in the troposphere decreases by over a factor of > 10 (compared to the summer). For this reason, total errors are typically slightly smaller in the winter.

The impact of thin clouds on the retrieval can result in RMS residuals of > 2 % in the spectral fits, reinforcing the requirement of the conservative cloud-filtering process. The impact of aerosols on the retrieval is similar (albeit smaller) and is discussed in more detail in Sect. 4. A perturbation method was used to assess the error associated with using the wrong a priori VMR profile shape of the target trace gas; VMR concentrations were perturbed 2 % at one altitude grid and the change in the retrieved total column was calculated. The largest changes in the retrieved total column occur from perturbations to the lowermost altitudes of the troposphere, indicating that E-AERI retrievals are dependent on the shape of the profile in the lower troposphere. This is discussed in more detail in Sect. 4. Table 2 lists the error components for each trace gas; retrievals performed on 4 April 2009 were used in the error analysis. The error bars in all graphs shown include all error sources (S_{tot}). Further error characteristics of the E-AERI can be found in Table 2 of Mariani et al. (2012).

AMTD
6, 547–586, 2013

4 2008–2009 trace gas measurements from the PEARL Ridge Lab

4.1 Comparisons of the E-AERI with other instruments

Clear-sky total columns of O_3, CO, CH_4, and N_2O from the PEARL Ridge Lab were retrieved using hourly-averaged E-AERI spectra (described in Sect. 2.1) and the SFIT2 emission add-on retrieval algorithm (described in Sects. 2.3, 3.1, and 3.2). These measurements at PEARL are not affected by local emissions of the Eureka weather station's power plant 15 km away. Figure 3 shows O_3, CO, CH_4, and N_2O total columns (from 0.610–100 km) measured at the PEARL Ridge Lab between September 2008 and October 2009. Also shown are measurements from the Bruker 125HR, Brewer, GBSs, and SAOZ spectrometers. Error bars are shown only for the E-AERI total columns for clarity. The pressure-temperature profiles and a priori VMR profiles for the E-AERI and 125HR are the same and SFIT2 was used to perform the retrievals for both instruments, making their measurements ideal for comparison purposes. Different retrieval algorithms and techniques were used for the Brewer, GBS, and SAOZ O_3 retrievals, as discussed in Sect. 2.4.

To compare the E-AERI data with the 125HR, a coincident time interval used the closest 125HR measurement recorded within three hours of an E-AERI measurement to maximize the number of coincident data points while minimizing the effect of measuring different air masses. All of the E-AERI and 125HR O_3 and CH_4 total column measurements agree within combined E-AERI and 125HR errors. For N_2O and CO, the agreement is slightly worse; 93 % and 90 % of the measurements, respectively, agree within combined errors. Comparisons between the two instruments can be quantified using the mean relative difference, which is the mean of the difference between the two instruments' measurements divided by their average, and the standard error on the mean, ($\sigma/\sqrt{N}$, where σ = standard deviation and N = number of data points). The mean relative differences (100 % × (E-AERI – instrument)/mean) between the E-AERI and the 125HR, Brewers, GBSs, and SAOZ are provided in Table 3. These differences are smaller than the total uncertainties (S_{tot}) of the E-AERI total column measurements

AMTD
6, 547–586, 2013

reported in Table 2, indicating good agreement. When the random error, S_m, is removed from S_{tot}, the differences are smaller than the uncertainty for all trace gases except CO. The larger difference for CO total columns is comparable to the differences (up to 17 %) found between AERI CO retrievals and convolved in-situ CO measurements by Yurganov et al. (2010), who attribute these discrepancies to the effect of aerosols on the measured radiances, which is not accounted for in their retrieval (nor in SFIT2). The largest differences seen in Fig. 3 occur in the summer months and are likely the result of increased H_2O and scattered solar energy from aerosols during this season. As H_2O increases in the atmosphere, significant broadening of H_2O emission lines occurs. The strong H_2O spectral lines dominate and interfere with the neighbouring spectral lines of the target trace gas, increasing the difficulty of distinguishing the emission signature of H_2O from that of the target trace gas. As a result, the H_2O concentration is over-estimated while the CO concentration is under-estimated for E-AERI CO retrievals in the summer. This is compounded by scattered solar energy from aerosols, which are not accounted for in SFIT2 and only have an impact in the summer months due to increased scattering via a higher solar elevation angle and increased aerosol particle size.

The seasonal cycle of O_3 (maximum in the late winter), driven by the Brewer-Dobson circulation, can be seen by the E-AERI, as is evident in Fig. 3. In addition, like the other spectrometers, the E-AERI observes a decrease in O_3 beginning in late February, which occurs as sunlight returns to Eureka. The seasonal cycle of CO (maximum in the winter) can also be observed, as previously demonstrated in Yurganov et al. (2010). Additional variation in the CO total column may be due to transport of biomass burning plumes and industrial emissions from lower latitudes to the Arctic (Stohl, 2006), with CO accumulating during the winter in the absence of OH oxidation. While most biomass burning events occur in the summer, dynamical transport from northern Eurasia into the polar dome occurs during the winter when only the E-AERI is operating (Stohl, 2006). E-AERI CH_4 and N_2O measurements are more variable than those measured with the 125HR, likely due to the E-AERI's high sensitivity to the surface concentration (whereas

AMTD
6, 547–586, 2013

the contribution of the surface concentration in the 125HR total column is diluted since the 125HR has greater vertical sensitivity which includes the stratosphere). The day-to-day variability in the CH_4 and N_2O column is greatest in the summer when the water vapour concentration is at a maximum, yet overall the measurements of CH_4 and N_2O remain relatively constant throughout the year, as expected.

There are two key differences between the E-AERI and the other ground-based spectrometers' measurements that can also contribute to the differences in Fig. 3. First, the E-AERI is zenith-viewing and samples air directly above PEARL, whereas the other spectrometers have different viewing geometries (as discussed in Sect. 2.4). Second, since the E-AERI measures thermal infrared emission, a sensitivity analysis indicates measured radiances are highly sensitive to the lower troposphere. This is also indicated in Mariani et al. (2012) and is evident in the seasonal cycle characteristic of tropospheric CO, as seen in Fig. 3. The other spectrometers are more sensitive to the stratosphere and thus to changes in the stratospheric concentration – for example, changes associated with chemical O_3 depletion. The E-AERI profile-scaled retrievals scale uniformly throughout the entire profile (the shape of the a priori profile cannot be altered), however, and are biased towards the concentration in the troposphere, contributing to the observed discrepancies.

The E-AERI and 125HR O_3 and CO measurements are highly correlated, as shown in Fig. 4, with a correlation coefficient of 0.92 and 0.95, respectively. As with the mean relative difference comparisons, a 3-h time interval was used to identify coincident measurements. E-AERI and Brewer, GBS, and SAOZ O_3 correlations (not shown) are not as strong (r = 0.70, 0.71, and 0.61, respectively), but given the different measurement techniques, this is expected. E-AERI and 125HR CH_4 and N_2O measurements are poorly correlated due to the lack of seasonal variability giving little dynamic range (not shown). E-AERI O_3 columns are typically greater than those measured by the 125HR by 7 % (averaged year-round), or by as much as 8–12 % in the summer. E-AERI CO columns are systematically smaller than those of the 125HR with a systematic bias of approximately −14 % (averaged year-round), or by as much as 10–27 % in the summer.

AMTD
6, 547–586, 2013

This bias accounts for the observed offset in the linear fit shown in Fig. 4b, which is very similar to the bias in the AERI vs. vertically averaged convolved in-situ CO measurements (∼ 13 %) in Yurganov et al., which has a comparable correlation ($m = 0.92$, $r = 0.76$). Since the mean relative error is larger than the error on that mean (i.e. larger than $3\sigma/\sqrt{N}$), the bias is statistically significant (Vigouroux et al., 2007). This indicates CO measurements from AERI instruments in general exhibit a systematic low-bias compared to in-situ and other remote sensing instruments.

4.2 Diurnal and seasonal cycles of CO

The ability of AERI systems to measure the seasonal and 24-h diurnal cycle of CO was demonstrated in Yurganov et al. (2010). The total column of CO is a minimum during sun-lit hours and a maximum during the night due to OH oxidation of CO, where OH is produced via photolysis. The 24-h diurnal cycle of CO for the entire year and for three different seasons experienced in the high Arctic can be seen in Fig. 5. The 24-h cycle of CO total column during polar night (22 October to 19 February) is compared to the 24-h cycle during polar day (22 April to 20 August) and the 24-h cycle during "equinoctial" months (March and September), which have roughly equal hours of sun and night in each day. As observed in the full year and equinoctial panels a and d, CO has a maximum around midnight due to the lack of OH oxidation (which is produced by photolysis) that occurs during the day. The 24-h diurnal cycle has an amplitude (maximum CO at night – minimum CO during the day/mean) of ∼ 6 % (indicated in panel a) for the full year; this is enhanced to ∼ 12 % (indicated in panel d) when filtered for the equinoctial months. Although the 24-h equinoctial cycle is more variable (larger error bars are due to the larger standard deviation), the amplitude is enhanced as expected, as this is the only time the Arctic receives roughly 12 h of sunlight each day. Note that more measurements were obtained during the polar night and equinoctial months compared to polar day, which has the adverse effect of biasing the full-year results. These amplitudes (∼ 6 and ∼ 12 %) are in good agreement with the ∼ 8 %

AMTD
6, 547–586, 2013

amplitude in the 24-h diurnal cycle of CO in Oklahoma found in Yurganov et al. (2010) and are the first measurements of this kind at Eureka.

The average CO total column during the equinoctial months is greater than the average CO during polar night due to the lifetime of CO (~ 2 months). Almost all measurements during the equinoctial period were taken in March, when the concentration of CO is at a maximum (as indicated in Fig. 3). Despite the sun's return in February, CO was built up during polar night and a lag between the sun's return and the depletion of CO due to OH oxidation occurs, resulting in the maximum occurring in March. Note that in order to quantify the impact of OH oxidation, the contribution from scattered solar energy by aerosols in the summer, which has a larger signature in the CO miniwindow, will have to be removed (future work).

The amplitude of the 365-day seasonal cycle of CO is much larger than the 24-h diurnal cycle. From Fig. 3, the amplitude of the seasonal cycle of CO is ~ 57 % (maximum CO in March – minimum CO in July/mean). As shown in Fig. 5, CO columns during polar day are ~ 46 % lower (indicated in panel c) than during polar night on average, consistent with the 24-h OH oxidation in the summer. These are the first measurements of the 365-day seasonal cycle of CO in the high Arctic performed by an FTIR. Both of these amplitudes are larger than that in Oklahoma (~ 40 %) (Yurganov et al., 2010), indicating a stronger 365-day seasonal cycle of CO at Eureka compared to mid-latitudes. Given the 24-h darkness followed by 24-h sunlight experienced in the Arctic, the increase in the amplitude of the 365-day seasonal cycle of CO is expected.

5 2011 trace gas measurements from 0PAL

Starting on 16 February 2011, the E-AERI resumed measurements closer to sea-level at 0PAL. The 600 m difference between the two sites has a large impact on the measured radiance, such as differences in the CO_2 band between 600–800 cm^{-1} due to a temperature inversion and – most notably – H_2O saturation (Mariani et al., 2012). Increased occurrence of clouds at lower altitudes also results in more spectra being

AMTD
6, 547–586, 2013

excluded due to cloud filtering. Depending on the season, 10–20 % of the water vapour column is located below 610 m, increasing the amount of H_2O interference with the target trace gas. Retrievals were performed using a total column from 0.010–100 km. To perform comparisons with total column measurements made from the PEARL Ridge Lab, the first 600 m of the E-AERI total columns were removed (the scaled VMR profile is on a 39-layer altitude grid; the lowest of which is 0.010–0.610 km) to match them with those measured at the Ridge Lab, effectively providing 0.610–100 km total columns. The additional error due to this removal is small (< 1 %) for all trace gases. The removal of the first 600 m has a large effect on tropospheric trace gas species, such as CO, which are heavily concentrated within the first 600 m (~ 20 %) compared to stratospheric species, such as O_3 (~ 0.6 % at Eureka).

Figure 6 shows measurements of total columns in 2011 of the same four trace gases shown in Fig. 3. Large gaps in the E-AERI data record are discussed in Sect. 2.1. The E-AERI total columns from 0PAL exhibit similar behaviour to those measured two years prior at the PEARL Ridge Lab, despite the additional water vapour. For instance, the seasonal cycle of CO can be resolved and the E-AERI CH_4 and N_2O total columns exhibit larger variability than the 125HR measurements, particularly in the summer. Persistent polar stratospheric clouds within the polar vortex resulted in severe chemical O_3 loss over Eureka in February and March 2011 (Manney et al., 2011; Adams et al., 2012b; Lindenmaier et al., 2012). This O_3 loss is observed by the E-AERI, although not to the same magnitude (due to the difference in vertical sensitivity). O_3 columns a week prior to the start of solar absorption measurements in 2011 are available from the E-AERI. All of the E-AERI O_3, CO, and CH_4 total columns agree within error with the 125HR measurements (96 % for N_2O).

The mean relative differences between the E-AERI and 125HR, Brewers, GBSs, and SAOZ for both 2008–2009 and 2011 are provided in Table 3. All mean relative differences are less than the uncertainties in the respective E-AERI total columns (see Table 2). Note that although the agreement in 2011 is better than in 2008–2009, the number of coincident measurements is significantly smaller for all trace gases, with

AMTD
6, 547–586, 2013

almost no coincident measurements occurring in the summer, where the largest discrepancies were observed in the 2008–2009 comparisons. Few ($N = 27$) coincident measurements between the E-AERI and the GBSs existed in 2011 (and no coincidences with the Brewers), likely attributing to worse agreement than in 2008–2009. The E-AERI O_3 measurements consistently have a positive bias compared to the 125HR, Brewers, and SAOZ throughout both measurement periods (2008–2009 and 2011), which is most prominent in the summer months (as with the 2008–2009 PEARL E-AERI retrievals). A negative bias relative to the GBSs is observed throughout both measurement periods, with very good agreement in 2008–2009.

As seen in Fig. 7, 2011 E-AERI and 125HR O_3 total column measurements are well correlated ($r = 0.74$), with weaker correlations between the E-AERI and the GBSs and SAOZ ($r = 0.43$ and 0.65, respectively). There were no coincident measurements between the E-AERI and Brewers during 2011. While the correlations are not as strong as for the 2008–2009 measurements from the PEARL Ridge Lab, this is likely due to the increase of aerosols at lower altitude (which is not accounted for in SFIT2), a smaller seasonal sampling range, and fewer coincident measurements in 2011 than for 2008–2009. As in 2008–2009, E-AERI O_3 columns are typically greater than the 125HR's (up to 5 %). 125HR CO measurements did not commence until later in the spring, when the E-AERI was not operating. For this reason, there were too few coincidences ($N = 4$) between the E-AERI and 125HR to accurately determine their CO correlation. CH_4 and N_2O measurements are poorly correlated due to the lack of seasonal variability (not shown). Despite the additional water vapour at 0PAL, based on the results in Table 3, E-AERI trace gas retrievals are comparable to those obtained at the PEARL Ridge Lab.

6 Conclusions

Total columns of O_3, CO, CH_4, and N_2O have been retrieved from October 2008 to September 2009 throughout polar night at the PEARL Ridge Lab and from February to December 2011 at 0PAL using a new version of the SFIT2 retrieval algorithm adapted

AMTD
6, 547–586, 2013

for infrared emission spectra. This is the first time infrared emission spectra have been used to retrieve trace gases using the newly modified version of SFIT2. The retrieval methodology described in this paper can be extended to all AERI instruments (of which more than 25 are in operation across the globe) and other spectrometers that measure infrared emission. This paper has also presented the first continuous polar night trace gas measurements at Eureka, which fill a gap in the PEARL dataset when the solar-viewing spectrometers are not operating. Obtaining continuous measurements of trace gases throughout polar night is valuable for long-term climatological studies of various trace gases as well as the determination of their seasonal variability.

Spectral fits indicate that SFIT2 is capable of accurately fitting the observed spectra, with RMS residuals < 1.5 %. The performance of the spectral fits is equivalent at 0PAL, where there is 10–20 % more water vapour. An error analysis has been performed, indicating that the uncertainty in the E-AERI total column measurements is 11.3 % for O_3, 14.7 % for CO, 11.0 % for CH_4, and 10.9 % for N_2O. E-AERI trace gas measurements agree well with those from the other spectrometers: mean relative differences are less than the uncertainties in the E-AERI total columns (1–14 % differences). The 2008–2009 E-AERI and 125HR measurements of O_3 and CO are highly correlated, with a correlation coefficient of $r = 0.92$ and 0.95, respectively, which is stronger than the O_3 correlations with the other spectrometers. The 2011 E-AERI 0PAL retrievals are comparable to those of 2008–2009, despite the increased water vapour at 0PAL. The E-AERI vs. 125HR CO correlation is comparable to the AERI vs. convolved in-situ CO correlation ($m = 0.92$, $r = 0.76$) found in Yurganov et al. (2010). The largest differences between the E-AERI and the other spectrometers for all four gases occur in the summer, indicating that the accuracy of the E-AERI's retrievals is season-dependent. This is likely due to the large ($\sim 10\times$) seasonal variability of water vapour in the high Arctic and scattered solar energy by aerosols in the summer which is not accounted for in SFIT2.

The budget of O_3 prior to, during, and after O_3 depletion events can be determined using E-AERI measurements. The 24-h diurnal cycle of CO has been resolved using

AMTD
6, 547–586, 2013

the E-AERI measurements, and the impact of OH oxidation on CO in the troposphere is observed in its total columns. The amplitude of the 24-h diurnal cycle of CO at Eureka as measured by the E-AERI is slightly greater (~ 12 %) than that in Oklahoma (~ 8 %) found using AERI CO retrievals (Yurganov et al., 2010). Similarly, the amplitude of the 365-day seasonal cycle of CO at Eureka is greater (~ 57 %) than that in Oklahoma (~ 40 %), indicating a stronger seasonal cycle of CO in the Arctic.

Retrievals of other trace gases, including CO_2, HCN, and C_2H_2 using E-AERI emission spectra are currently being evaluated. Along with CO, the E-AERI's year-round measurements of these trace gases can provide insight when investigating biomass burning events. Although the frequency of biomass burning events is decreased in the winter, the E-AERI is the only instrument at Eureka capable of measuring emission products during this time when dynamical transport to the Arctic is enhanced, lengthening the potential period of studying such events. E-AERI retrievals can also be performed on a per-spectrum basis (every 7 min) as opposed to hourly-averaged in order to investigate the dynamical transport of trace gases (for instance, measuring the variability of CO as a proxy of vertical motion above Eureka). Ongoing measurements of the trace gases discussed in this paper from 0PAL are being conducted (with no measurement interruptions since November 2011) to investigate their diurnal and interanual variability and for satellite validation. E-AERI trace gas measurements will continue to be used to fill the polar night gap in the PEARL dataset, providing insight into the state of the atmosphere year-round.

Acknowledgements. The Polar Environment Atmospheric Research Laboratory (PEARL) is operated by the Canadian Network for the Detection of Atmospheric Change (CANDAC). CANDAC/PEARL funding partners are: the Arctic Research Infrastructure Fund, Atlantic Innovation Fund/Nova Scotia Research Innovation Trust, Canadian Foundation for Climate and Atmospheric Science, Canadian Foundation for Innovation, Canadian Space Agency (CSA), Environment Canada (EC), Government of Canada International Polar Year, Natural Sciences and Engineering Research Council (NSERC), Ontario Innovation Trust, Ontario Research Fund, Indian and Northern Affairs Canada, and the Polar Continental Shelf Program. Spring visits to PEARL were made as part of the Canadian Arctic ACE Validation Campaigns, led by Kaley

AMTD
6, 547–586, 2013

A. Walker and supported by CSA, EC, NSERC and the Northern Student Training Program. Thanks to David Hudak at Environment Canada for providing MMCR data. Thanks to PEARL site manager Pierre Fogal and CANDAC operators Ashley Harrett, Alexei Khmel, Paul Loewen, Oleg Mikhailov, Keith MacQuarrie and Matt Okraszewski who have helped with the P-AERI and E-AERI measurements at PEARL. Thanks to Stephane Lantagne and Guillaume Gamache from ABB for their work installing the E-AERI, Dan Weaver for his help with water vapour data, and Simone Chaudhary for her help with automating SFIT2. Thanks also to the staff at the Eureka Weather Station for their support and hospitality.

References

Adams, C., Strong, K., Batchelor, R. L., Bernath, P. F., Brohede, S., Boone, C., Degenstein, D., Daffer, W. H., Drummond, J. R., Fogal, P. F., Farahani, E., Fayt, C., Fraser, A., Goutail, F., Hendrick, F., Kolonjari, F., Lindenmaier, R., Manney, G., McElroy, C. T., McLinden, C. A., Mendonca, J., Park, J.-H., Pavlovic, B., Pazmino, A., Roth, C., Savastiouk, V., Walker, K. A., Weaver, D., and Zhao, X.: Validation of ACE and OSIRIS ozone and NO_2 measurements using ground-based instruments at 80° N, Atmos. Meas. Tech., 5, 927–953, doi:10.5194/amt-5-927-2012, 2012a.

Adams, C., Strong, K., Zhao, X., Bassford, M. R., Chipperfield, M., Daffer, W., Drummond, J. R., Farahani, F., Feng, W., Fraser, A., Goutali, F., Manney, G., McLinden, C., Pazmino, A., Rex, M., and Walker, K.: Severe 2011 ozone depletion assessed with 11 years of ozone, NO_2, and OClO measurements at 80° N, Geophys. Res. Lett., 39, L05806, doi:10.1029/2011GL050478, 2012b.

Batchelor, R., Strong, K., Lindenmaier, R., Mittermeier, R., Fast, H., Drummond, J. R., and Fogal, P.: A New Bruker IFS 125HR FTIR Spectrometer for the Polar Environment Atmospheric Research Laboratory at Eureka, Nunavut, Canada: measurements and comparison with the existing Bomem DA8 Spectrometer, Atmos.-Ocean. Tech., 26, 1328–1340, 2009.

Batchelor, R. L., Kolonjari, F., Lindenmaier, R., Mittermeier, R. L., Daffer, W., Fast, H., Manney, G., Strong, K., and Walker, K. A.: Four Fourier transform spectrometers and the Arctic polar vortex: instrument intercomparison and ACE-FTS validation at Eureka during the IPY springs of 2007 and 2008, Atmos. Meas. Tech., 3, 51–66, doi:10.5194/amt-3-51-2010, 2010.

AMTD
6, 547–586, 2013

Becker, E. and Notholt, J.: Ground based FTIR-emission spectroscopy of the polar atmosphere during the wintertime, Proceedings of SPIE, 3106, 154–158, 1997.

Bianchini, G., Cortesi, U., and Carli, B.: Emission Fourier transform spectroscopy for remote sensing of the Earth's atmosphere, Ann. Geophys., 46, 205–222, 2003, http://www.ann-geophys.net/46/205/2003/.

Bianchini, G., Palchetti, L., Muscari, G., Fiorucci, I., Di Girolamo, P., and Di Iorio, T.: Water vapor sounding with the far infrared REFIR-PAD spectroradiometer from a high-altitude ground-based station during the ECOWAR campaign, J. Geophys. Res., 116, D02310, doi:10.1029/2010JD014530, 2010.

Fast, H., Mittermeier, R., and Makino, Y.: A ten-year record of Arctic trace gas total column measurements at Eureka, Canada, from 1997 to 2006, Atmos.-Ocean, 49, 67–94, 2011.

Fisher, H. and Oelhaf, H.: Remote sensing of vertical profiles of atmospheric trace constituents with MIPAS limb-emission spectrometers, Appl. Optics, 35, 2787–2796, 1996.

Fraser, A., Adams, C., Drummond, J. R., Goutail, F., Manney, G., and Strong, K.: The Polar Environment Atmospheric Research Laboratory UV-visible Ground-Based Spectrometer: first measurements of O_3, NO_2, BrO, and OClO columns, J. Quant. Spectrosc. Ra., 110, 986–1004, 2009.

Hase, F., Hannigan, J. W., Coffey, M. T., Goldman, A., Hopfner, M., Jones, N. B., Rinsland, C. P., and Wood, S. W.: Inter-comparison of retrieval codes used for the analysis of high-resolution, ground-based FTIR measurements, J. Quant. Spectrosc. Ra., 87, 25–52, 2004.

Hendrick, F., Pommereau, J.-P., Goutail, F., Evans, R. D., Ionov, D., Pazmino, A., Kyrö, E., Held, G., Eriksen, P., Dorokhov, V., Gil, M., and Van Roozendael, M.: NDACC/SAOZ UV-visible total ozone measurements: improved retrieval and comparison with correlative ground-based and satellite observations, Atmos. Chem. Phys., 11, 5975–5995, doi:10.5194/acp-11-5975-2011, 2011.

International Organization of Standardization: Guide to the Expression of Uncertainty in Measurement, 1st edn., US Government Printing Office, Washington, 101 pp., 1993.

Lam, K. S., Savastiouk, V., Fung, W., Chan, T., and Lamb, K.: Recalculation of 11-year total ozone of Brewer spectrophotometer 115, J. Geophys. Res., 112, D15104, doi:10.1029/2006JD008178, 2007.

Lindenmaier, R.: Studies of Arctic Middle Atmospheric Chemistry using Infrared Absorption Spectroscopy, PhD thesis, University of Toronto, 308 pp., 2012.

AMTD
6, 547–586, 2013

Lindenmaier, R., Batchelor, R., Strong, K., Fast, H., Goutail, F., Kolonjari, F., McElroy, C. T., Mittermeier, R., and Walker, K.: An evaluation of infrared microwindows for ozone retrievals using the Eureka Bruker 125HR Fourier transform spectrometer, J. Quant. Spectrosc. Ra., 111, 569–585, 2010.

Lindenmaier, R., Strong, K., Batchelor, R. L., Chipperfield, M. P., Daffer, W. H., Drummond, J. R., Duck, T. J., Fast, H., Feng, W., Fogal, P. F., Kolonjari, F., Manney, G. L., Manson, A., Meek, C., Mittermeier, R. L., Nott, G. J., Perro, C., and Walker, K. A.: Unusually low ozone, HCl, and HNO_3 column measurements at Eureka, Canada during winter/spring 2011, Atmos. Chem. Phys., 12, 3821–3835, doi:10.5194/acp-12-3821-2012, 2012.

Manney, G., Santee, M., Rex, M., Livesey, N., Pitts, M., Veefkind, P., Nash, E., Wohltmann, I., Lephmann, R., Froidevaux, L., Poole, L., Schoeberl, M., Haffner, D., Davies, J., Dorokhov, V., Gernandt, H., Johnson, B., Kivi, R., Kyro, E., Larsen, N., Levelt, P., Makshtas, A., McElroy, C. T., Nakajima, H., Parrondo, M., Tarasick, D., Gathen, P., Walker, K. A., and Zinoviev, N.: Unprecedented Arctic ozone loss in 2011, Nature, 478, 469–475, 2011.

Mariani, Z., Strong, K., Wolff, M., Rowe, P., Walden, V., Fogal, P. F., Duck, T., Lesins, G., Turner, D. S., Cox, C., Eloranta, E., Drummond, J. R., Roy, C., Turner, D. D., Hudak, D., and Lindenmaier, I. A.: Infrared measurements in the Arctic using two Atmospheric Emitted Radiance Interferometers, Atmos. Meas. Tech., 5, 329–344, doi:10.5194/amt-5-329-2012, 2012.

Meier, A., Goldman, A., Manning, P. S., Stephen, T. M., Rinsland, C. P., Jones, N. B., and Wood, S. W.: Improvements to air mass calculations for ground-based infrared measurements, J. Quant. Spectrosc. Ra., 83, 109–113, 2004.

Platt, U. and Stutz, J.: Differential Optical Absorption Spectroscopy, edited by: Guzzi, R., Lanzerotti, L. J., Imboden, D., and Platt, U., Springer, Germany, 175–285, 2008.

Pommereau, J. P. and Goutail, F.: O_3 and NO_2 ground-based measurements by visible spectrometry during Arctic winter and spring 1988, Geophys. Res. Lett., 15, 891–894, 1988.

Pougatchev, N., Connor, B., and Rinsland, C.: Infrared measurements of the ozone vertical distribution above Kitt Peak, J. Geophys. Res., 100, 16689–16697, doi:10.1029/95JD01296, 1995.

Raffalski, U., Hochschild, G., Kopp, G., and Urban, J.: Evolution of stratospheric ozone during winter 2002/2003 as observed by a ground-based millimetre wave radiometer at Kiruna, Sweden, Atmos. Chem. Phys., 5, 1399–1407, doi:10.5194/acp-5-1399-2005, 2005.

AMTD
6, 547–586, 2013

Ravishankara, A. R., Daniel, J. S., and Portmann, R. W.: Nitrous oxide (N_2O): the dominant ozone-depleting substance emitted in the 21st century, Science, 326, 123–125, 2009.
Rinsland, C. P., Jones, N., Connor, B., Logan, J., Pougatchev, N., Goldman, A., Murcray, F., Stephen, T., Pine, A., Zander, R., Mahieu, E., and Demoulin, P.: Northern and Southern Hemisphere ground-based infrared spectroscopic measurements of tropospheric carbon monoxide and ethane, J. Geophys. Res., 103, 28197–28217, 1998.
Rodgers, C. D.: Retrieval of atmospheric temperature and composition from remote measurements of thermal radiation, Rev. Geophys., 14, 609–624, 1976.
Rodgers, C. D.: Characterization and error analysis of profiles retrieved from remote sounding measurements, J. Geophys. Res., 95, 5587–5595, 1990.
Rodgers, C. D.: Inverse methods for atmospheric sounding: theory and practice, in: Series on Atmospheric, Oceanic and Planetary Physics, Vol. 2, World Scientific Publishing Co. Pte. Ltd., New Jersey, 2000.
Rodgers, C. D. and Connor, B. J.: Intercomparison of remote sounding instruments, J. Geophys. Res., 108, 4116, 1–14, 2003.
Rothman, L. S., Gordon, I. E., Barbe, A., Benner, D. C., Bernath, P. F., Birk, M., Boudon, V., Brown, L. R., Camparague, A., Champion, J.-P., Chance, K., Coudert, L. H., Dana, V., Devi, V. M., Fally, S., Flaud, J.-M., Gamache, R. R., Goldman, A., Jacquemart, D., Kleiner, I., Lacome, N., Lafferty, W. J., Mandin, J.-Y., Massie, S., Mikhailenko, S. N., Miller, C. E., Moazzen-Ahmadi, M., Naumenko, O. V., Nikitin, A. V., Orphal, J., Perevalov, V. I., Perrin, A., Predoi-Cross, A., Rinsland, C., Rotger, M., Simeckova, M., Smith, M., Sung, K., Tashkun, S. A., Tennyson, J., Vandaele, A. C., Toth, R., and Vander Auwera, J.: The HITRAN 2008 molecular spectroscopic database, J. Quant. Spectrosc. Ra., 110, 533–572, 2009.
Savastiouk, V. and McElroy, C. T.: Brewer spectrophotometer total ozone measurements made during the 1998 Middle Atmosphere Nitrogen Trend Assessment (MANTRA) campaign, Atmos.-Ocean, 43, 315–324, 2005.
Stohl, A.: Characteristics of atmospheric transport into the Arctic atmosphere, J. Geophys. Res., 111, D11306, doi:10.1029/2005JD006888, 2006.
Stremme, W., Krueger, A., Harig, R., and Grutter, M.: Volcanic SO_2 and SiF_4 visualization using 2-D thermal emission spectroscopy – Part 1: Slant-columns and their ratios, Atmos. Meas. Tech., 5, 275–288, doi:10.5194/amt-5-275-2012, 2012.
Vigouroux, C., De Mazière, M., Errera, Q., Chabrillat, S., Mahieu, E., Duchatelet, P., Wood, S., Smale, D., Mikuteit, S., Blumenstock, T., Hase, F., and Jones, N.: Comparisons between

AMTD
6, 547–586, 2013

ground-based FTIR and MIPAS N_2O and HNO_3 profiles before and after assimilation in BASCOE, Atmos. Chem. Phys., 7, 377–396, doi:10.5194/acp-7-377-2007, 2007.

Waldmann, I., Tinetti, G., Drossart, P., Swain, M., Deroo, P., and Griffith, C.: Ground-based near infrared emission spectroscopy of HD 189733B, Astrophys. J., 744, 35, doi:10.1088/0004-637X/744/1/35, 2012.

Warneke, C., Froyd, K., Brioude, J., Bahreini, R., Brock, C., Cozic, J., de Gouw, J., Fahey, D., Ferrare, R., Holloway, J., Middlebrook, A., Miller, L., Montzka, S., Schwartz, J., Sodermann, H., Spackman, J., and Stohl, A.: An important contribution to springtime Arctic aerosol from biomass burning in Russia, Geophys. Res. Lett., 37, L01801, doi:10.1029/2009GL041816, 2010.

Yurganov, L., McMillan, W., Wilson, C., Fischer, M., Biraud, S., and Sweeney, C.: Carbon monoxide mixing ratios over Oklahoma between 2002 and 2009 retrieved from Atmospheric Emitted Radiance Interferometer spectra, Atmos. Meas. Tech., 3, 1319–1331, doi:10.5194/amt-3-1319-2010, 2010.

AMTD
6, 547–586, 2013

Table 1. Retrieval specifications for each target trace gas: the retrieval miniwindow (spectral range), interfering species scale-fitted in each miniwindow, SNR, and typical RMS residual of the spectral fit for spectra measured in the spring (April).

Trace Gas	Miniwindow (cm^{-1})	Interfering Species	SNR	Typical RMS (%)
O_3	950–1100	H_2O, CO_2, O_3^{667}, O_3^{676}, O_3^{686}, O_3^{668}	20	1.5
CO	2000–2200	O_3, N_2O, H_2O, OCS	70	1.4
CH_4	1150–1229	SO_2, H_2O, HDO, O_3, CCl_2F_2, HNO_3, CH_3D, N_2O	75	1.2
N_2O	1160–1300	CH_4, SO_2, H_2O, HDO, O_3, CCl_2F_2, HNO_3, CH_3D	85	1.5

AMTD
6, 547–586, 2013

Table 2. Error components for each retrieved trace gas total column. S_{tot} is determined from Eq. (4). Errors are based on a single spectrum on 4 April 2009; these errors are typical for other dates and decrease slightly in the winter and increase slightly in the summer as a result of decreased/increased H_2O emission.

Trace Gas	S_m (%)	S_s (%)	S_{temp} (%)	S_{lint} (%)	S_{lwidth} (%)	S_{intret} (%)	$S_{intspec}$ (%)	S_{tot} (%)
O_3	1.1	6.1	8.7	2.9	0.5	0.01	1.4	11.3
CO	8.0	11.9	3.4	0.2	0.1	0.01	0.1	14.7
CH_4	6.0	8.2	3.3	2.2	0.4	0.01	0.2	11.0
N_2O	6.5	6.7	4.7	2.6	0.5	0.02	0.5	10.9

AMTD
6, 547–586, 2013

Table 3. O_3, CO, CH_4, and N_2O total column comparisons between the E-AERI and the 125HR, Brewers, GBSs, and SAOZ for 2008–2009 and 2011. The Brewers, GBSs, and SAOZ cannot measure CO, CH_4, and N_2O. The mean relative difference (100 % × (E-AERI – instrument)/mean) is given with the standard error ($\sigma/\sqrt{N}$) and the number of coincident data points (N) in brackets.

		Mean relative difference with the E-AERI (%)			
Year	Trace Gas	125HR	Brewers	GBSs	SAOZ
2008–2009	O_3	7.7 ± 0.3 (437)	9.9 ± 1.6 (137)	−2.9 ± 1.0 (222)	8.4 ± 0.9 (188)
	CO	−14.4 ± 1.4 (402)	–	–	–
	CH_4	2.0 ± 0.3 (474)	–	–	–
	N_2O	−1.2 ± 0.4 (514)	–	–	–
2011	O_3	8.1 ± 1.0 (123)	N/A (0)	−9.4 ± 1.2 (27)	7.4 ± 1.9 (144)
	CO	−1.9 ± 0.6 (4)	–	–	–
	CH_4	−1.2 ± 1.4 (144)	–	–	–
	N_2O	−2.1 ± 0.9 (132)	–	–	–

AMTD
6, 547–586, 2013

Fig. 1. Satellite composite image of Eureka on Ellesmere Island (insert: highlighted in red), Nunavut, Canada in the early summer. The PEARL Ridge Lab and 0PAL are separated by 15 km and their locations are indicated on the image. Image: © 2012 Google, © 2012 Tele Atlas, © 2012 Wikipedia.

AMTD
6, 547–586, 2013

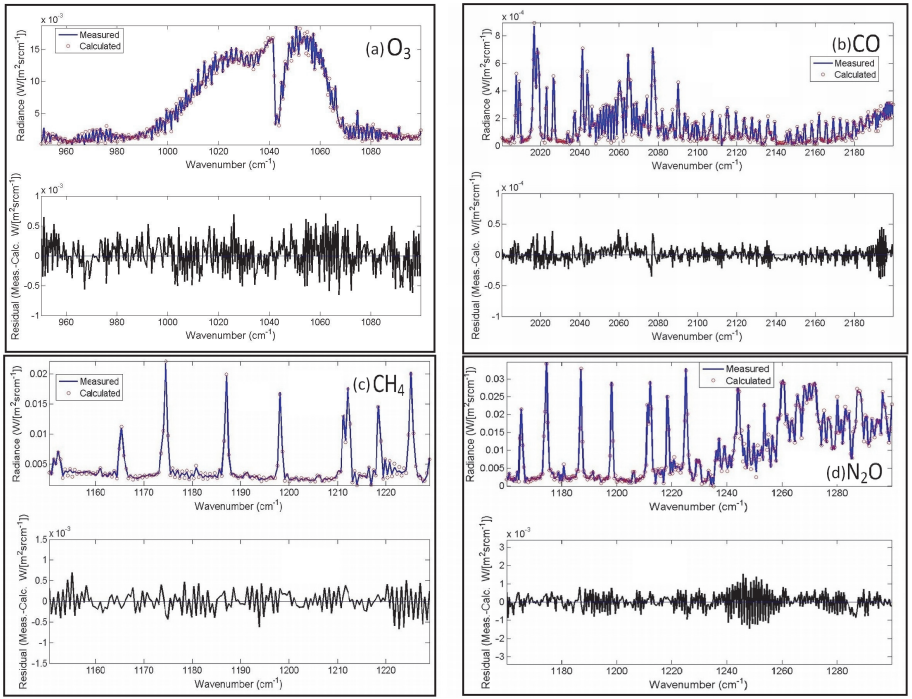

Fig. 2. Samples of spectral fits for retrievals of **(a)** O_3, **(b)** CO, **(c)** CH_4, and **(d)** N_2O. Top panels show the measured (blue) and fitted spectra (red circles), with their residuals shown in the bottom panels. Note the vertical scales of the two panels are different (residuals are zoomed-in). Retrievals were performed on 4 April 2009 using SFIT2 and hourly-averaged E-AERI spectra.

AMTD
6, 547–586, 2013

Arctic polar night retrievals of trace gases using the E-AERI

Z. Mariani et al.

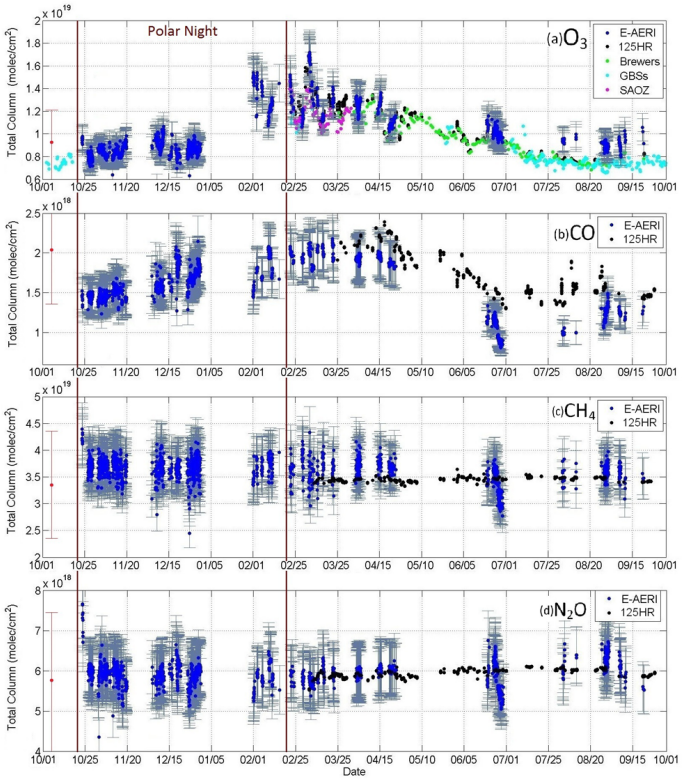

Fig. 3. Total column measurements of **(a)** O_3, **(b)** CO, **(c)** CH_4, and **(d)** N_2O from the PEARL Ridge Lab. Dates are given as MM/DD from 2008–2009. E-AERI (blue), 125HR (black), three Brewers (green), two GBSs (cyan), and the SAOZ (pink) measurements are shown for comparison. Error bars are shown only for the E-AERI for clarity. The a priori column is shown for one day (red) with error bars equivalent to $\mathbf{S}_a$. Polar night is indicated between the brown vertical lines.

AMTD
6, 547–586, 2013

Arctic polar night retrievals of trace gases using the E-AERI

Z. Mariani et al.

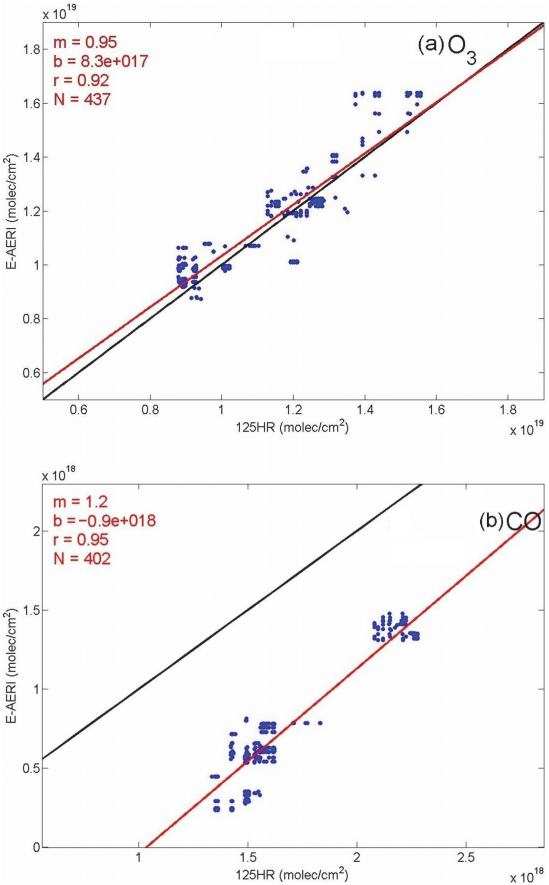

Fig. 4. Total column comparisons for E-AERI vs. 125HR **(a)** O_3 and **(b)** CO using a 3-h coincidence criterion. The black line indicates the 1 : 1 line, the red line indicates the linear fit (m = fitted slope, b = fitted y-intercept, r = Pearson product-moment correlation coefficient, N = number of coincidences).

AMTD
6, 547–586, 2013

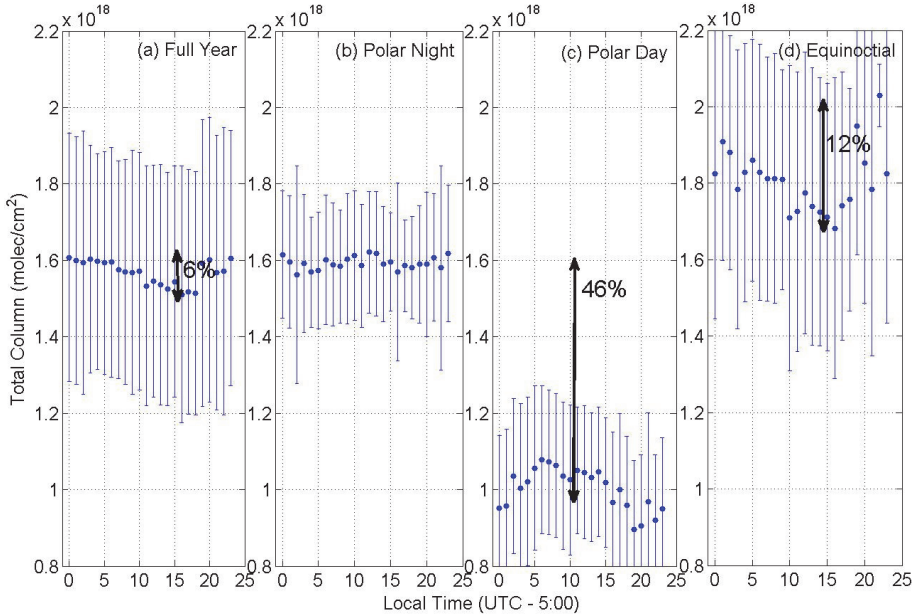

Fig. 5. 24-h diurnal cycle of CO during each season as measured by the E-AERI during 2008–2009: **(a)** averaged across the full year, **(b)** averaged during polar night (no sun), **(c)** averaged during polar day (only sun), and **(d)** March and September averaged during ~ 12 h of sunlight (equinoctial). Error bars represent the standard deviation of the hourly means.

AMTD
6, 547–586, 2013

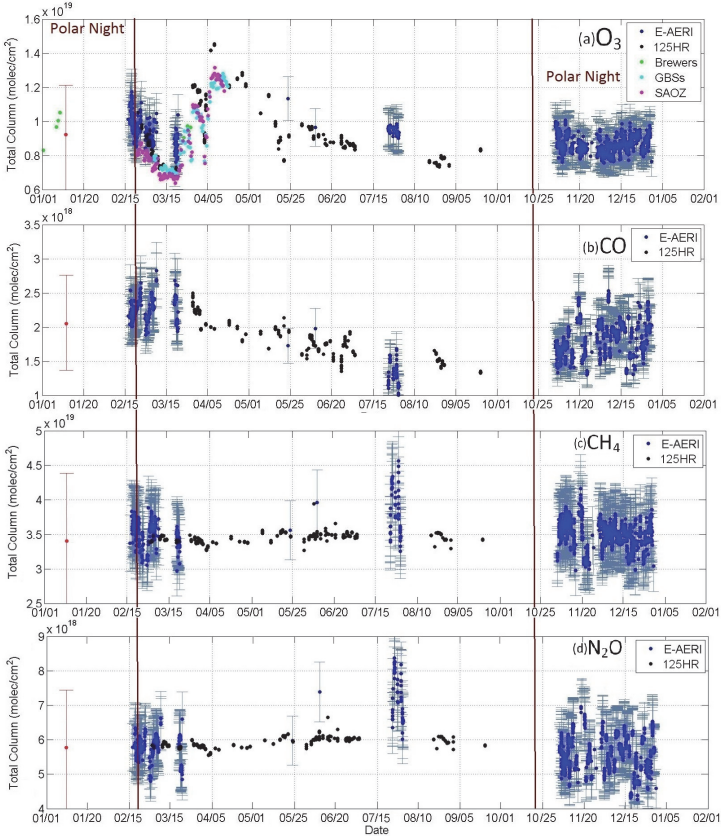

Fig. 6. Same as in Fig. 3, except for 2011. The E-AERI was located at 0PAL (10 m altitude), while the other spectrometers were located at the PEARL Ridge Lab (610 m altitude). The a priori column is shown for one day (red) with error bars equivalent to $\mathbf{S}_a$. Polar night is indicated outside the brown vertical lines.

AMTD
6, 547–586, 2013

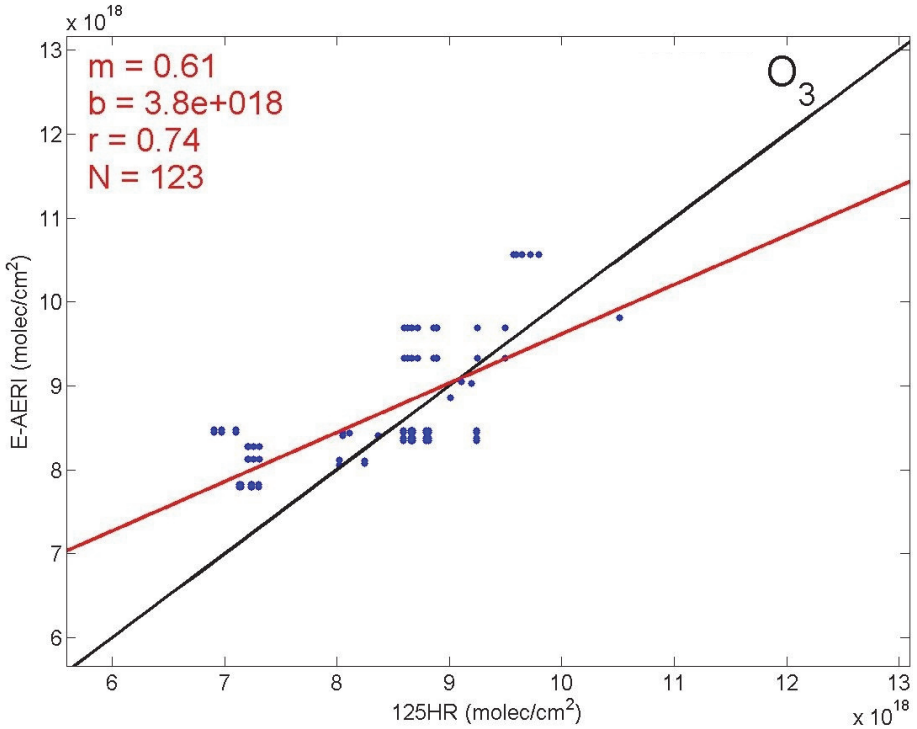

Fig. 7. O_3 total column comparisons for E-AERI vs. 125HR using a 3-h coincidence criterion. The black line indicates the 1 : 1 line, the red line indicates the linear fit (m = fitted slope, b = fitted y-intercept, r = Pearson product-moment correlation coefficient, N = number of coincidences).

AMTD
6, 547–586, 2013